Check for updates

From ECHo-1k to ECHo-100k:Optimization of High-Resolution Metallic Magnetic Calorimeters with Embedded ^{163}Ho for Neutrino Mass Determination

M. Griedel[1] · F. Mantegazzini[1] · A. Barth[1] · E. Bruer[1] · W. Holzmann[1] ·
R. Hammann[1] · D. Hengstler[1] · N. Kovac[1] · C. Velte[1] · T. Wickenhäuser[1] ·
A. Fleischmann[1] · C. Enss[1] · L. Gastaldo[1] · H. Dorrer[2] · T. Kieck[3] · N. Kneip[3] ·
Ch. E. Düllmann[2,4,5] · K. Wendt[3]

Abstract

The ECHo experiment aims at determining the effective electron neutrino mass by analyzing the endpoint of the ^{163}Ho electron capture spectrum. High energy resolution detectors with a well-tailored detector response are the essential ingredient for the success of the ECHo experiment. Metallic magnetic calorimeter arrays enclosing ^{163}Ho have been chosen for the ECHo experiment. The first MMC array, ECHo-1k, showed excellent performances with an average energy resolution of 5.5 eV FWHM @ 5.9 keV. Based on the results obtained with the ECHo-1k array, optimization studies have paved the way towards a new detector design for the next experimental phase, ECHo-100k. The ECHo-100k chip features an optimized single pixel design to improve the detector performance as well as an upgraded on-chip thermalization layout. The newly fabricated ECHo-100k detectors have been fully characterized at room temperature, at 4 K and at millikelvin temperature. The obtained results show that the ECHo-100k array achieved the expected performance with an average energy resolution of 3.5 eV FWHM @ 5.9 keV, fulfilling the requirements for the ECHo-100k experimental phase.

Keywords MMC · ECHo · LTD · Electron neutrino · ^{163}Ho · Electron capture

✉ M. Griedel
griedel@kip.uni-heidelberg.de

✉ F. Mantegazzini
federica.mantegazzini@kip.uni-heidelberg.de

Extended author information available on the last page of the article

1 Introduction

The Electron Capture in ^{163}Ho (ECHo) experiment aims to reach sub-eV sensitivity on the effective electron neutrino mass analyzing the calorimetrically measured electron capture (EC) spectrum of ^{163}Ho. The detector technology used consists of metallic magnetic calorimeter (MMC) arrays implanted with ^{163}Ho, which allow for an excellent energy-resolution, a fast response and a quantum efficiency close to 100% [1]. MMCs exploits the temperature dependence of a paramagnetic material sitting in a static magnetic field to detect small deviations from the equilibrium temperature of about 20 mK due to the particle interactions. The ECHo schedule currently foresees two phases: A small scale experiment, ECHo-1k, with about 100 pixels to reach a sensitivity below 20 eV on the neutrino mass and a medium scale experiment, ECHo-100k, which will lower the sensitivity below 2 eV. The modular approach of the ECHo experiment will also allow for scaling up to further phases with larger number of pixels. The main goal of the detector optimization for ECHo-1k was the achievement of an average energy resolution below 10 eV FWHM for MMC pixels containing ^{163}Ho. An average energy resolution of 5.5 eV FWHM by measureing the N1 line at 400 eV was demonstrated over 43 pixels, fulfilling the mentioned requirement [2]. The results obtained during the ECHo-1k phase were used as a base to optimize the detector design and layout to meet the more challenging requirements for the next phase, ECHo-100k, with an energy resolution below 5 eV FWHM. The planned total ^{163}Ho activity during the ECHo-100k phase is 100 kBq, which will be reached using about 12,000 MMC detector pixels with an ^{163}Ho activity of about 10 Bq/pixel. To operate such a high number of detectors in parallel, a multiplexed read-out is necessary which is currently being developed [3].

2 The ECHo-100k Detector Design

The detector chip designed and fabricated for the ECHo-100k phase is a detector array with 64 MMC pixels based on the double-meander design [4]. The single pixel is composed of two gold absorber layers, inside which the ^{163}Ho source is embedded, a paramagnetic Ag:Er sensor in a constant magnetic field and a weak thermal link to a thermal bath. The sensor is thermally tightly connected to the absorber. A superconducting coil is used both for providing the constant magnetic field, which is produced by a persistent current injected into the coil, and as a pick-up coil for the detection of the magnetization change in the sensor following a change of temperature of the detector. Between the sensor layer and the absorber layer three stem structures are introduced to minimize the contact area and to prevent athermal phonons from travelling through the sensor and releasing the energy in the substrate. Figure 1 *right* shows a blow-up scheme of the single pixel layout.

Each pair of pixels share the same read-out channel and therefore the chip can be read out by 32 SQUID channels. Two detector channels (i.e. two pairs of
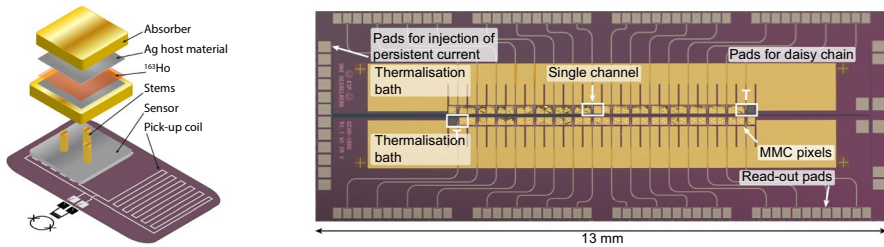
Fig. 1 *left* Schematic layout of a single detector channel made of two MMC pixels. *right* ECHo-100k array chip with 32 MMC channels. Each single detector channel consist of two MMC pixels. The gold thermalization baths and the read-out pads are highlighted. (Color figure online.)

pixels), placed at two opposing corners of the array, have only one wing of the double-meander equipped with the Ag:Er paramagnetic sensor and gold absorber and they are dedicate to temperature monitoring. These channels are not meant to be implanted with ^{163}Ho. The remaining 60 pixels form 30 gradiometric channels which are insensitive to common change of temperature. In total, 23 channels will have both pixels implanted with ^{163}Ho and seven channels will have only one pixel enclosed with the ^{163}Ho source, allowing for *in situ* background measurements. Figure 1 *left* shows the ECHo-100k chip after fabrication. The ECHo-100k detector chip is compatible both with dc-SQUID read-out and multiplexing read-out [2].

Single-Pixel Design The single-pixel geometry has been optimized to minimize the detector heat capacity and therefore to enlarge the signal amplitude and to improve the energy resolution. For that, the absorber thickness has been optimized on the basis of Monte Carlo simulations and theoretical calculations of photon transport in gold, to ensure on one side a negligible escape loss and on the other side the minimal absorber heat capacity. The chosen design value is 3.0 μm for each absorber layer. The volume of the sensor is adjusted such that the heat capacity of the sensor matches the heat capacity of the absorber (including the contribution from the implanted ^{163}Ho), this leads to optimal detector performances at 20 mK [5].

Implantation ^{163}Ho is embedded inside the detector pixels via ion implantation at the RISIKO facility at Mainz University [6]. The detector chip is prepared by depositing a photoresist mask on the single chip leaving open only the implantation areas of 150 μm on top of each absorber. The mask is designed such that no ^{163}Ho ions are implanted in the absorber volume directly above the stem structures, minimizing the probability that phonons travel to the sensor through the stems, causing a potential loss of signal. A thin silver layer of typically 100 nm is then sputter-deposited on the full chip as host material for ^{163}Ho. In addition, the continuous silver layer is also contacted to ground to compensate the potential charging of implanted ions. About a day after ion implantation, a second thin silver layer of typically 100 nm is deposited additionally over the sample. Finally, the photoresist mask is lifted off and a second photoresist mask is prepared for the structuring of the second absorber layer with an area of 165 × 165 μm, which consists of further 3 μm of gold to fully enclose the ^{163}Ho source.

Chip Layout The chip layout is characterized by a compact geometry for highly efficient [163]Ho implantation. During the implantation process, the absorber array is scanned with an ion-beam and the [163]Ho ions are directly implanted into the whole scanned area. Thus, after implantation, [163]Ho is present also in the host material layer that covers the regions in between the implantation areas. In order to reduce the amount of [163]Ho that is wasted in first place during the implantation process, the space between the implantation areas should be minimized. Hence, the ECHo-100k design features a compact pixel arrangement, as visible in Fig. 1. The width of the MMC array is 0.43 mm while the size of the ion-beam is about 0.7 mm. Furthermore, the on-chip circuitry offers the possibility to simultaneously inject the persistent current in all the pixels of one chip or in multiple chips at once. Finally, the layout of the bond-pads allows to connect the ECHo-100k chip both to dc-SQUID read-out chips and SQUID microwave multiplexing read-out chips.

Thermalization The on-chip thermalization layout has been optimized with respect to the detector chip developed for the ECHo-1k experimental phase. In the ECHo-1k design each group of four MMC pixels is connected to one gold area, itself is linked to the next one via gold bond-wires. The final gold area is significantly larger and is positioned at the edge of the chip, to be finally connected to the copper holder to which the chip is glued. An innovative solution implemented in the ECHo-100k design consists in connecting each pair of MMC pixels to a gold area that is linked to the consecutive one via gold air bridges that are structured during the microfabrication process.

3 Characterization of the ECHo-100k Detector

3.1 Characterization of a Not Implanted ECHo-100k Chip

Several not-implanted ECHo-100k detector chips have been tested at room temperature, at 4 K and at millikelvin temperature. At room temperature the resistances of the superconducting lines and of the heater-switch used for the injection of the persistent current have been measured. At 4 K the functionality of the heater-switch has been tested and the inductance of the meander-shaped pick-up coil has been measured, giving a value of $L_m = 2.1 \pm 0.2$ nH. This matches the expected value from the design, $L_{m,theo} = 2.27$ nH. At millikelvin temperature the detector array has been fully characterized by means of an external [55]Fe source and a dc-SQUID-based readout, testing the simultaneous injection of the persistent current in all the detector pixels, measuring the signal amplitude as a function of temperature and the energy resolution per pixel.

Comparing the room temperature tests with the results achieved at millikelvin temperature, it was possible to demonstrate a correlation which allows to reliably predict the functionality of the chip at millikelvin from the resistance values measured at room temperature. This strategy is crucial to test detectors on wafer scale before proceeding with the [163]Ho implantation.
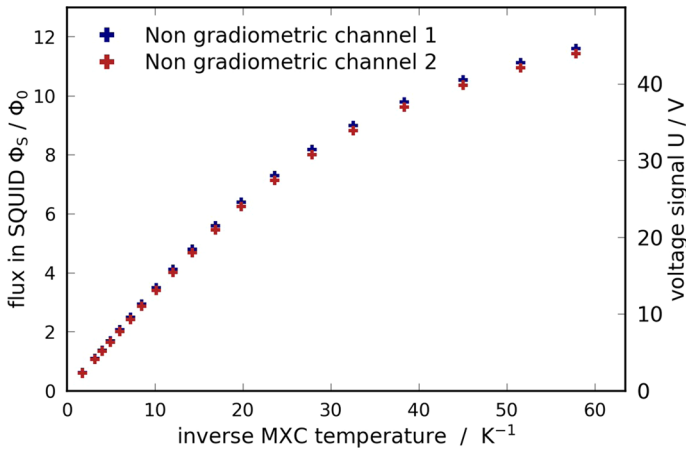
Simultaneous Current Injection

Fig. 2 Magnetization measurement for both non-gradiometric channels as function of inverse temperature for a persistent current of 40 mA. The *left* axis shows the magnetization signal as flux in the SQUID. The *right* right axis shows the magnetization as the proportional voltage signal from the SQUID. (Color figure online.)
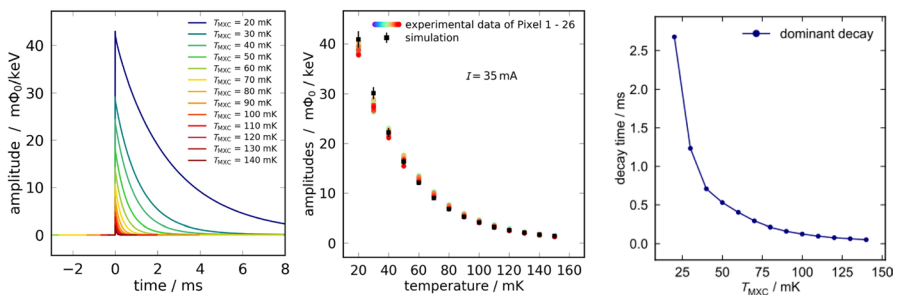

Fig. 3 *left* Pulse shape of the ^{55}Fe Kα line at different temperatures. *middle* Experimental signal amplitudes scaling with temperature compared to the signal amplitude dependence of temperature from simulation (*black squares*). *left* Dominant decay time at different temperatures. (Color figures online.)

To test the simultaneous current injection into all the detector pixels on the chip, the temperature dependence of the magnetization response is measured in both non-gradiometric channels present on the chip. As shown in Fig. 2 the magnetization curves agree for both the non-gradiometric channels. Since the two channels are positioned on opposite sides of the detector chip, we can conclude that the simultaneous current injection works as expected over the complete chip.

Temperature Dependence of the Signal Amplitude The detector response corresponding to the Kα photons from the ^{55}Fe calibration source has been measured in a temperature range between 20 and 140 mK (Fig. 3 *left*). The signal amplitude is determined by two crucial properties of MMCs, namely heat capacity and magnetisation, and it is expected to decrease with increasing temperature [5]. The measured amplitudes as a function of temperature agree with the expectations based on the
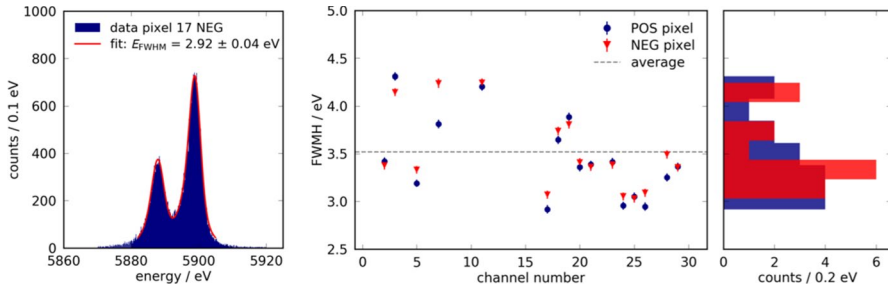
Fig. 4 *left* Fit of the ^{55}Fe Kα line of one pixel. *right* Energy resolution (FWHM) per pixel, POSP and NEGP denotes the polarity of the pixels in one channel. The average value is indicated with the *grey dashed line*. (Color figure online.)

detector simulations, as shown in Fig. 3 *middle*. The signal decay can be described by a sum of exponential functions due to the step structure of the thermal link to the on-chip thermal bath. In first approximation, it depends on the detector heat capacity and on the thermal conductance G of the thermal link to the bath: $\tau \approx C_{tot}/G$. The decay becomes faster because the thermal conductance to the bath G increases faster with temperature then the heat capacity. This dependence of the decay on the temperature is shown in Fig. 3 *right*.

Energy Resolution The energy resolution per pixel has been estimated fitting the measured ^{55}Fe Kα lines with a convolution of the intrinsic line shape [7] and the Gaussian detector response, as shown in Fig. 4 *left*.

The energy resolution is given as the FWHM of the Gaussian broadening derived from the fit. The resulting energy resolution values per pixel are summarized in Fig. 4 *right*. The average energy resolution is 3.5 ± 0.4 eV FWHM @ 5.9 keV, which is consistent with the expectations. Therefore, the newly designed chip fulfils the requirement for the ECHo-100k phase. The limit on the energy resolution given by thermodynamic noise of the detector is estimated to be below 1 eV FWHM @ 5.9 keV and the achieved energy resolution is limited by the readout noise level, which leaves room for further improvements.

3.2 Characterization of the Implanted ECHo-100k Chip

A first ECHo-100k chip has been implanted with a goal activity of about 3 Bq and characterized in terms of ^{163}Ho activity per pixel and energy resolution. For a first control of the activity per pixel, the second part of the absorber was not micro-fabricated on top of the implanetd absorber area. The ^{163}Ho activity is estimated from the time difference between two consecutive events in the same pixel $\delta\Delta T_{pixel}$. A histogram of ΔT_{pixel} is fitted with an exponential, from which the activity can be extracted. Figure 5 shows the resulting activity map, with an activity per pixel between 1.71 Bq and 3.24 Bq.

The energy resolution of the implanted pixels has been extracted from a fit of the NI line at 400 eV using a convolution of a Lorentzian line shape and the Gaussian
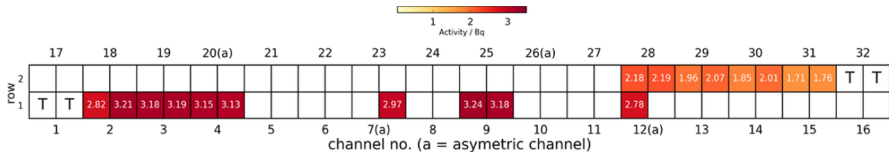
Fig. 5 Activity map of the first implanted ECHo-100k chip. The *white* pixels were not measured. (Color figure online.)

Activity map (Activity / Bq):

row	17	18	19	20(a)	21	22	23	24	25	26(a)	27	28	29	30	31	32
row 2								2.18	2.19	1.96	2.07	1.85	2.01	1.71	1.76	T · T
row 1	T	T	2.82	3.21	3.18	3.19	3.15	3.13		2.97		3.24	3.18		2.78	

| 1 | 2 | 3 | 4 | 5 | 6 | 7(a) | 8 | 9 | 10 | 11 | 12(a) | 13 | 14 | 15 | 16 |

channel no. (a = asymetric channel)

Fig. 6 Fit of the high energy part of the ^{163}Ho N1 line with a convolution of a Lorentzian and a Gaussian detector response for one pixel. (Color figure online.)
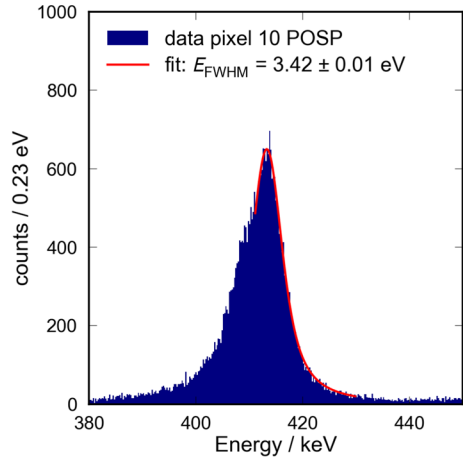
detector response[1], an example is shown in Fig. 6. The resulting energy resolution is below 5 eV FWHM for all measured pixels, matching the goal for this experimental phase. Since the first fabricated ECHo-100k chip was only equipped with the first absorber layer, a small and therefore negligible error on the energy resolution is expected. In fact, the heat capacity at 20 mK of a pixel is $C_{tot} = 2.03$ pJ/K, while the contribution of the heat capacity from the second absorber layer is only $C_{a2} = 0.13$ pJ/K, from calculations. The energy resolution scales with $\sim \sqrt{C_{tot}}$, therefore the contribution from the missing absorber layer can be neglected.

4 Conclusion

A new metallic magnetic calorimeter array has been designed and fabricated for the ECHo-100k experimental phase, which aims to reach a sensitivity below 2 eV on the effective electron neutrino mass. The single chip layout is optimized to reach an excellent energy resolution and the on-chip thermalization ensures a reliable detector response. The implantation procedure has been developed and tested. The new detector array has been tested and fully characterized, especially in terms of detector

---

[1] The actual line shape is complex and contains multiple contributions [8]. Only the high-energy part of the line is fitted. For the current resolution this part can still be modelled with a convolution of a Gaussian and Lorentzian distribution.

response as a function of temperature, energy resolution and ^{163}Ho activity per pixel. The positive results, with an energy resolution well below 5 eV FWHM, from fitting the ^{163}Ho N1-line at 400 eV, and a ^{163}Ho activity up to 3.24 Bq/pixel, match the expectations and set the starting point of the ECHo-100k phase.

References

1. L. Gastaldo et al., Eur. Phys. J. Spec. Top. **226**, 1623–1694 (2017). https://doi.org/10.1140/epjst/e2017-70071-y
2. F. Mantegazzini et al., Metallic magnetic calorimeter arrays for the first phase of the ECHo experiment. NIM A **1030**, 166406 (2021)
3. M. Wegner et al., J. Low Temp. Phys. **193**, 462 (2018). https://doi.org/10.1007/s10909-018-1878-3
4. A. Fleischmann et al., AIP Conf. Proc. **1185**, 571–78 (2009). https://doi.org/10.1063/1.3292407
5. A. Fleischmann, C. Enss, G.M. Seidel, Top. Appl. Phys. **99**, 151–216 (2005)
6. T. Kieck et al., Nucl. Inst. Meth. A **945**, 162602 (2019). https://doi.org/10.1016/j.nima.2019.162602
7. G. Hoelzer et al., Phys. Rev. A **56**, 4554–4568 (1997). https://doi.org/10.1103/PhysRevA.56.4554
8. M. Brass, M. Haverkort, New J. Phys. **22**, 093018 (2020). https://doi.org/10.1088/1367-2630/abac72

Publisher's Note Springer Nature remains neutral with regard to jurisdictional claims in published maps and institutional affiliations.

Authors and Affiliations

M. Griedel[1] [ORCID] **· F. Mantegazzini[1] · A. Barth[1] · E. Bruer[1] · W. Holzmann[1] · R. Hammann[1] · D. Hengstler[1] · N. Kovac[1] · C. Velte[1] · T. Wickenhäuser[1] · A. Fleischmann[1] · C. Enss[1] · L. Gastaldo[1] · H. Dorrer[2] · T. Kieck[3] · N. Kneip[3] · Ch. E. Düllmann[2,4,5] · K. Wendt[3]**

1   Kirchhoff-Institute for Physics, Heidelberg University, Im Neuenheimerfeld 227, 69120 Heidelberg, Germany

2　　Department of Chemistry - TRIGA Site, Johannes Gutenberg University Mainz, Fritz-Strassmann-Weg 2, 55128 Mainz, Germany

3　　Institute of Physics, Johannes Gutenberg University Mainz, Staudingerweg 7, 55128 Mainz, Germany

4　　GSI Helmholtzzentrum für Schwerionenforschung GmbH, Planckstraße 1, 64291 Darmstadt, Germany

5　　Helmholtz Institute Mainz, Staudingerweg 18, 55128 Mainz, Germany